JOURNAL OF PROPULSION AND POWER
Vol. 18, No. 1, January–February 2002

Thermodynamic Cycle Analysis of Pulse Detonation Engines

William H. Heiser*
U.S. Air Force Academy, Colorado 80840
and
David T. Pratt†
University of Washington, Seattle, Washington 98195

Pulse detonation engines (PDEs) are currently attracting considerable research and development attention because they promise performance improvements over existing airbreathing propulsion devices. Because of their inherently unsteady behavior, it has been difficult to conveniently classify and evaluate them relative to their steady-state counterparts. Consequently, most PDE studies employ unsteady gasdynamic calculations to determine the instantaneous pressures and forces acting on the surfaces of the device and integrate them over a cycle to determine thrust performance. A classical, closed thermodynamic cycle analysis of the PDE that is independent of time is presented. The most important result is the thermal efficiency of the PDE cycle, or the fraction of the heating value of the fuel that is converted to work that can be used to produce thrust. The cycle thermal efficiency is then used to find all of the traditional propulsion performance measures. The benefits of this approach are 1) that the fundamental processes incorporated in PDEs are clarified; 2) that direct, quantitative comparisons with other cycles (e.g., Brayton or Humphrey) are easily made; 3) that the influence of the entire ranges of the main parameters that influence PDE performance are easily explored; 4) that the ideal or upper limit of PDE performance capability is quantitatively established; and 5) that this analysis provides a basic building block for more complex PDE cycles. A comparison of cycle performance is made for ideal and real PDE, Brayton, and Humphrey cycles, utilizing realistic component loss models. The results show that the real PDE cycle has better performance than the real Brayton cycle only for flight Mach numbers less than about 3, or cycle static temperature ratios less than about 3. For flight Mach numbers greater than 3, the real Brayton cycle has better performance, and the real Humphrey cycle is an overoptimistic (and unnecessary) surrogate for the real PDE cycle.

Nomenclature

C_p	=	constant-pressure specific heat capacity, Btu/lbm · °R (kJ/kg-K)
F	=	thrust, lbf (N)
f	=	mass fuel–air ratio
g_c	=	gravitational constant, 32.174 lbm · ft/lbf · s^2 (1 kg-m/N · s^2)
g_0	=	standard acceleration of gravity, 32.174 ft/s^2 (9.8067 m/s^2)
h_{PR}	=	lower heating value of fuel, Btu/lbm (kJ/kg)
I_{sp}	=	specific impulse, s
M	=	Mach number
$\dot{m}$	=	mass-flow rate, lbm/s (kg/s)
p	=	static pressure, lbf/ft^2 (N/m^2)
q	=	heat added or rejected, Btu/lbm (kJ/kg)
$\tilde{q}$	=	nondimensional heat added, q/C_pT
S	=	specific fuel consumption, lbm/s · lbf (mg/N · s)
s	=	specific entropy, Btu/lbm · °R (kJ/kg-K)
T	=	static temperature, °R (K)
V	=	velocity, ft/s (m/s)
γ	=	ratio of specific heats
η	=	efficiency
π_c	=	compression static pressure-rise ratio, p_3/p_0
ψ	=	compression static temperature-rise ratio, T_3/T_0

Subscripts

b	=	burner (combustion) process
CJ	=	Chapman–Jouguet state
c	=	compression process
e	=	expansion process
tc	=	thermodynamic cycle
th	=	thermal
X	=	isentropic end state in Fig. 11
Y	=	isentropic end state in Fig. 11
0	=	freestream

I. Introduction

PULSE detonation propulsion (PDP) and pulse detonation engines (PDEs) are currently attracting considerable attention because they promise performance improvements over existing airbreathing propulsion devices, especially at low flight Mach numbers.[1,2] Because of their inherently unsteady behavior, it is difficult to classify and evaluate them relative to their steady-state counterparts.

Most PDE/PDP studies employ unsteady gasdynamic calculations to determine the instantaneous pressures and forces acting on the surfaces of the device and integrate them over a cycle to determine thrust performance.[3–5] These studies require considerable finite element or finite volume modeling and computational effort and are not well suited to discovering basic conceptual truths. This study was, therefore, motivated by the desire to find a simpler approach that would expose the underlying physics and provide direct, transparent results.

The approach chosen was classical, thermodynamic closed-cycle analysis because it is treated comprehensively in the literature[6–8] and is familiar to most aerospace engineers and scientists. It is also clear that, because the function of all chemical propulsion engines is to convert the heating value (heat of reaction) of combustion of fuel with air into exhaust flow kinetic energy, they can be treated as thermodynamic devices. The consequences of this choice can be fairly judged by what follows.

Received 16 September 2000; revision received 27 May 2001; accepted for publication 20 July 2001.

*Professor of Aeronautics Emeritus. Fellow AIAA.
†Professor of Mechanical Engineering Emeritus. Associate Fellow AIAA.

II. Ideal Thermodynamic Cycle Analysis

This study begins with classical, ideal, closed-cycle thermodynamic analysis because it contains all of the necessary elements and will easily be extended to include real effects (losses). The study follows the PDE and Brayton (turbojet, ramjet) cycles in parallel to capitalize on the communal understanding of the latter and to provide a reasonable basis of comparison for the PDE as an alternative propulsion cycle to a turbojet. The Humphrey cycle is included because it is often cited as having similar performance to the PDE. As ever, the approximations resulting from assuming thermodynamic equilibrium, employing calorically perfect gases of constant properties, replacing chemical reactions with heat addition but no mass addition, and employing perfect processes are more than compensated for by the instructive value of the results. Fixed reference values are assumed, specifically the ratio of specific heats $\gamma = 1.4$, freestream static temperature $T_0 = 400^\circ$R (222 K), and the mass-specific constant-pressure specific heat capacity $C_p = 0.24$ Btu/lbm $\cdot\,^\circ$R (1.00 kJ/kg $\cdot$ K). Although these values are used throughout, the equations are constructed to allow any fixed values to be assumed.

A. Ideal Brayton Cycle

The ideal Brayton cycle is shown in the T–s (temperature–entropy) diagram of Fig. 1, where conventional nomenclature and station numbering have been used. The sequential processes are described as follows[8]:

From point 0 to point 3 indicates the adiabatic, isentropic compression from the freestream static temperature T_0 to the combustor entry static temperature T_3. This compression can be accomplished by various combinations of freestream deceleration (from point 0 to point 2) and mechanical compression (from point 2 to point 3), as in any turbojet engine. The cycle static temperature ratio T_3/T_0 is a primary thermodynamic quantity that appears frequently in cycle analyses. We will follow Builder[6] and denote this important ratio $\psi \equiv T_3/T_0$. As a practical matter, the velocity of the flow entering the combustor is reduced as much as possible to improve the conditions for burning and to reduce friction and Rayleigh losses. T_3 is, therefore, nearly the stagnation temperature of the flow.

From point 3 to point 4 indicates the constant static pressure, frictionless heat addition from the combustor entry static temperature T_3 to the combustor exit static temperature T_4. The Gibbs equation for a calorically perfect gas can be directly integrated to determine the entropy increase resulting from q_{add}, the heat added per unit mass of air entering the combustor.

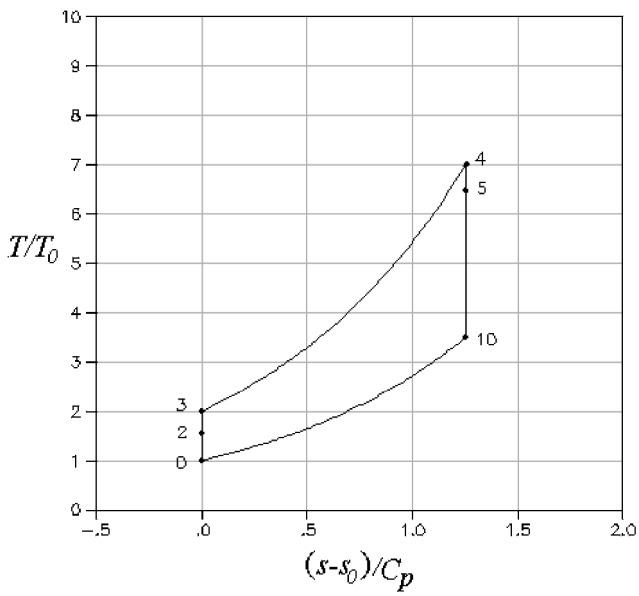

Fig. 1 Temperature–entropy diagram for the ideal Brayton cycle for $\psi \equiv T_3/T_0 = 2$ and $\tilde{q} \equiv fh_{\text{PR}}/C_pT_0 = 5$.

From point 4 to point 10 indicates the adiabatic, isentropic expansion from the combustor exit static pressure p_4 to the freestream static pressure $p_{10} = p_0$. This expansion includes the mechanical extraction of the energy required for the earlier mechanical compression (from point 4 to point 5), as well as the acceleration of the flow to high velocity (from point 5 to point 10), as in any turbojet engine.

From point 10 to point 0, the thermodynamic cycle is closed via an imagined constant static pressure, frictionless process in which sufficient heat is rejected to the surroundings from the exhaust flow to return it to its original thermodynamic state. Specifically, the amount of heat rejected per unit mass of air processed q_{rej} must reduce the entropy from point 10 to point 0 an equal amount to the entropy increase from point 3 to point 4. Interestingly, control volume analysis of this process reveals that the velocity (and kinetic energy) of the flow remains constant,[8] and, hence, the magnitude of the velocity that produces thrust is unambiguous. Most important, the heat rejected is equivalent to that portion of the heat added that is not converted to exhaust kinetic energy.

The cycle thermal efficiency η_{th} is defined as the ratio of external work done by the cycle to the heating value supplied by the fuel q_{supp}, whereas the thermodynamic cycle efficiency η_{tc} is defined as the ratio of external work done by the cycle to the thermal energy actually absorbed by (added to) the working substance in the cycle q_{add} (Ref. 8). Because all component processes in the ideal cycle are assumed to be without loss, $q_{\text{add}} = q_{\text{supp}}$, and, consequently, $\eta_{\text{th}} = \eta_{\text{tc}}$ for all ideal cycles.

For the ideal thermodynamic cycle, the thermal efficiency is given by

$$\eta_{\text{th}} \equiv \frac{q_{\text{add}} - q_{\text{rej}}}{q_{\text{add}}} = 1 - \frac{q_{\text{rej}}}{q_{\text{add}}} \tag{1}$$

where $q_{\text{add}} = q_{\text{supp}}$ is the product of the mass fuel–air ratio f and the fuel lower heating value h_{PR}, and the rejected heat is obtained from

$$\begin{aligned} q_{\text{rej}} &= h_{10} - h_0 = C_p(T_{10} - T_0) \\ &= C_pT_0(T_{10}/T_0 - 1) = C_pT_0(T_4/T_3 - 1) \\ &= (C_pT_0/T_3)(T_4 - T_3) = (h_4 - h_3)/\psi = q_{\text{add}}/\psi \end{aligned} \tag{2}$$

There follows immediately the familiar classical result for an ideal Brayton cycle,

$$\eta_{\text{th}} = 1 - (1/\psi) \tag{3}$$

Note that, for the ideal Brayton cycle, the thermodynamic cycle efficiency is not a function of the heat added, but only of the cycle static temperature ratio ψ, and it increases monotonically with increasing ψ to an asymptotic limit, $\eta_{\text{th}} \to 1$ as $\psi \to \infty$.

B. Ideal PDE Cycle

Except for the heat addition (combustion) process, which requires further elaboration, the thermodynamic cycle for an ideal PDE cycle is identical to that of the ideal Brayton cycle. The reader's attention is, therefore, directed to the pulse detonation wave process. The reader is advised that the ensuing mathematical analyses will be straightforward and is, therefore, is encouraged to focus on the physical phenomena involved.

From point 3 to point 4, the generally accepted model of a normal detonation wave in PDP devices is seen, namely, that of a Zeldovich/von Neumann/Doering (ZND) wave.[2,9] This is a compound wave consisting of a normal shock wave progressing into the undisturbed fuel–air mixture, which is nearly at rest at the combustor entry condition (point 3), followed by release of sensible heat in a constant-area region (Rayleigh flow) terminating at point 4. The strength (Mach number, pressure ratio, or temperature ratio) of the leading shock wave, from point 3 to point 3a, is uniquely determined by the initial conditions and the amount of heat added. The entire process is constrained by the Chapman–Jouguet condition, which requires that the local Mach number at the termination of the heat addition region (point 4) be one (sonic or choked flow). The heat addition region is followed by a very complex constant-area region of

nonsteady expansion waves, the most important property of which is that they are assumed to be isentropic. This ZND wave structure is stationary in detonation wave coordinates from the undisturbed flow to the end of the heat addition process. To ensure the greatest cycle performance, it is further assumed that 1) the nonsteady expansion (from point 4 to point 10) of the detonated mixture is isentropic, 2) every fluid particle experiences the same normal detonation process, and 3) there is no energy penalty to the cycle for whatever spark or ignition torch may be required to initiate the detonation process.

The T–s diagram for the PDE cycle may now be constructed. In doing so, note that the T–s diagram portrays the sequence of states through which the working fluid passes, rather than, for example, a history of what happens at some location or across some component. This may be counter-intuitive to those whose experience with steady-flow devices has conditioned them to associate state properties with engine positions, but it will be familiar to those who have performed air-standard cycle analysis of intermittent combustion engines based on, for example, the Otto and Diesel cycles.

Consider carefully the presumed point 4–point 10 isentropic expansion process of the PDE cycle. To the best of our knowledge, no simple devices have been proposed that can take all fluid elements generated by the PDE heating/combustion process isentropically to local atmospheric pressure and, hence, to their ideal exhaust kinetic energy and velocity. The special challenge presented by unsteady devices is that the fluid elements have their static properties distributed in space and time, and each must, therefore, be given individual treatment. Contrast this with the steady-state Brayton cycle, where the uniformity of the heating/combustion products allows a simple nozzle to expand them to local atmospheric pressure. This highlights the important fact that invention is required to allow the PDE to achieve its potential and that this is a worthy, if not essential, area of study. Nevertheless, the upper limit of performance will be established by presuming that ideal expansion is possible. Any likelihood that this approach should be regarded as excessively optimistic is countered by thermodynamic cycle analysis making the ideal performance unambiguous and, thus, that it establishes an upper bound of performance against which proposed ingenious solutions to the expansion problem may be judged.

The PDE cycle T–s diagram that conforms to the description given is shown in Fig. 2. The slight downturn in the process isoline just before point 4 corresponds to the familiar situation near Mach 1 where heat addition causes the static temperature to drop.[10] Note that the entropy generated in the detonation wave heat addition process is the sum of that generated in the point 3–point 3a adiabatic normal shock wave and that generated in the point 3a–point 4 constant-area heat addition process that follows. This is the entropy increase that must be removed in the point 10–point 0 heat rejection process to close the cycle.

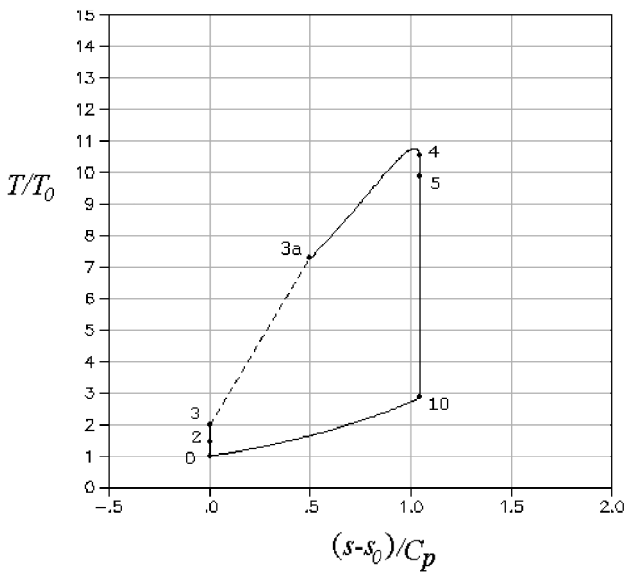

Fig. 2 Temperature–entropy diagram for the ideal PDE cycle for $\psi = 2$ and $\tilde{q} = 5$.

This approach takes advantage of entropy being a thermodynamic state property, independent of velocity reference frame, as opposed to, for example, the total pressure and total temperature.

Closed-form algebraic solutions for the leading normal shock wave (Chapman–Jouguet) Mach number and the entropy rise in the detonation wave have been derived by Shapiro[10] and others[9,11] and are given, respectively, by

$$M_{\mathrm{CJ}}^2 = (\gamma+1)(\tilde{q}/\psi) + 1 + \sqrt{[(\gamma+1)(\tilde{q}/\psi)+1]^2 - 1} \tag{4}$$

where $\tilde{q} \equiv q_{\mathrm{supp}}/C_pT_0 = fh_{\mathrm{PR}}/C_pT_0$, and

$$\frac{s_4 - s_3}{C_p} = -\ell n\left[M_{\mathrm{CJ}}^2\left(\frac{\gamma+1}{1+\gamma M_{\mathrm{CJ}}^2}\right)^{(\gamma+1)/\gamma}\right] \tag{5}$$

Consequently, the constant-pressure heat rejected and the cycle thermal efficiency become

$$q_{\mathrm{rej}} = h_{10} - h_0 = C_p(T_{10} - T_0) = C_pT_0\left[\exp\left(\frac{s_{10}-s_0}{C_p}\right) - 1\right]$$

$$= C_pT_0\left[\exp\left(\frac{s_4 - s_3}{C_p}\right) - 1\right]$$

$$= C_pT_0\left[\frac{1}{M_{\mathrm{CJ}}^2}\left(\frac{1+\gamma M_{\mathrm{CJ}}^2}{\gamma+1}\right)^{(\gamma+1)/\gamma} - 1\right] \tag{6a}$$

$$\eta_{\mathrm{th}} = 1 - \left[\frac{1}{M_{\mathrm{CJ}}^2}\left(\frac{1+\gamma M_{\mathrm{CJ}}^2}{\gamma+1}\right)^{(\gamma+1)/\gamma} - 1\right]\Big/\tilde{q} \tag{6b}$$

C. Ideal Humphrey Cycle

Finally, the analysis of an ideal Humphrey cycle is included because it has been frequently employed as a surrogate for the PDE cycle for the purpose of estimating the cycle thermal efficiency.[1,4] It is not required for one to understand PDE cycle performance, but it is included here for historical completeness so that the reader may judge the accuracy or utility of employing this approximation.

The Humphrey cycle may be considered a modification to the Brayton cycle in which the constant-pressure heat addition process is replaced by a constant-volume heat addition process. Using the same analysis procedures and assumptions as the preceding derivations, the reader may readily verify that the thermal efficiency of the ideal Humphrey cycle is given by

$$\eta_{\mathrm{th}} = 1 - (1/\tilde{q})[(1+\gamma\tilde{q}/\psi)^{1/\gamma} - 1] \tag{7}$$

The T–s diagram for the ideal Humphrey cycle is presented in Fig. 3, together with the PDE and Brayton cycles drawn from Figs. 1 and 2, respectively. It is apparent from a comparative inspection of the three ideal cycles displayed in Fig. 3 that the thermal efficiency of the ideal Humphrey cycle is close to, but always somewhat less than, that of the ideal PDE cycle. Note also that, as was the case for the ideal Brayton cycle, the thermodynamic cycle efficiency for the ideal Humphrey cycle, given by Eq. (7), increases monotonically with increasing ψ to an asymptotic limit, $\eta_{\mathrm{th}} \to 1$ as $\psi \to \infty$ for any finite value of $\tilde{q}$.

D. Ideal Propulsion Engine Performance

Once the cycle thermal efficiency is known, standard, one-dimensional models of engine thrust[7,8] may be employed to determine the more traditional uninstalled performance measures, such as the specific thrust $F/\dot{m}_0$ (thrust per unit mass flow rate of air), specific fuel consumption S (mass flow rate of fuel per unit thrust), and specific impulse I_{sp} (thrust per unit weight flow rate of fuel). In these models, it is assumed that the mass flow of fuel is negligible compared to that of the air, that every element of the exhaust flow is

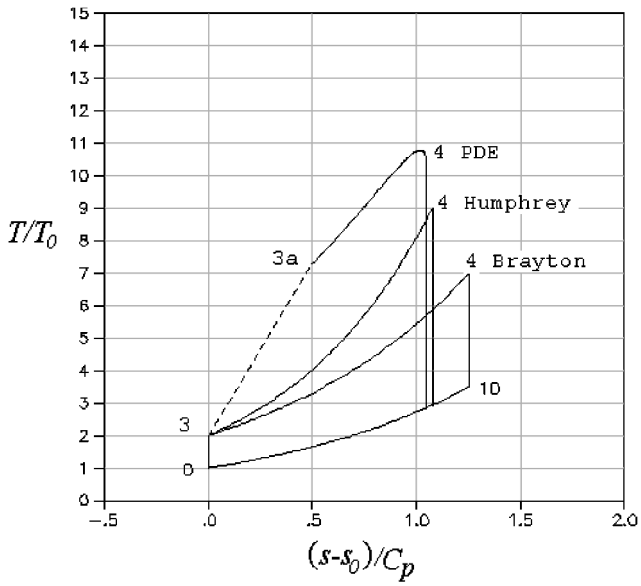

Fig. 3 Temperature–entropy diagrams for the ideal PDE, Brayton, and Humphrey cycles for $\psi = 2$ and $\tilde{q} = 5$.

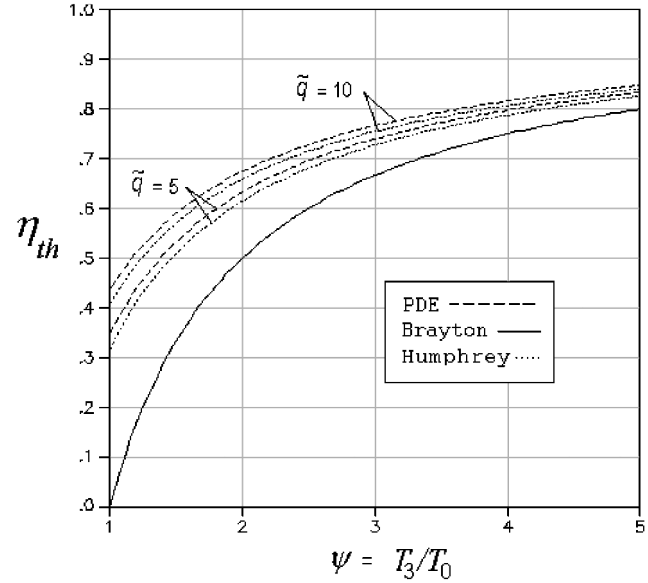

Fig. 4 Thermal efficiency η_{th} of ideal PDE, Brayton, and Humphrey cycles as functions of ψ for $\tilde{q} = 5$ and 10.

perfectly expanded to match the local ambient static pressure, and that there is no installation drag.

These performance measures are

$$F/\dot{m}_0 \equiv 1/g_c\left[\sqrt{V_0^2 + 2\eta_{\text{th}} q_{\text{supp}}} - V_0\right] \tag{8}$$

$$S \equiv \dot{m}_f/F = f\dot{m}_0/F = f/(F/\dot{m}_0) \tag{9}$$

$$I_{\text{SP}} \equiv F/\dot{w}_f = g_c/g_0 S \tag{10}$$

In Eqs. (8–10), V_0 is the velocity of the vehicle; f is the mass fuel–air ratio; $q_{\text{supp}} \equiv f h_{\text{PR}}$ is the heat supplied by the fuel per unit mass-flow rate of air, where h_{PR} is the (lower) heating value of the fuel; and g_c and g_0 are the gravitational constant and the standard acceleration of gravity, respectively.

Note that all propulsion engine performance measures depend directly on the cycle thermal efficiency, so that all comparisons could be made solely on the basis of that quantity. Propulsion engine performance measures are, therefore, included here only as a sanity check for comparison with normal experience.

E. Ideal Thermodynamic Cycle Analysis Results

Because ideal Brayton cycle behavior depends only on ψ, and ideal PDE and Humphrey cycle behavior depend only on ψ and $\tilde{q}$, it follows that the behavior of every imaginable ideal PDE, ideal Brayton, and ideal Humphrey device is as represented in Fig. 4.

Figure 4 demonstrates that both the ideal PDE and Humphrey cycles enjoy a significant cycle thermal efficiency advantage over the ideal Brayton cycle when $1 < \psi < 3$, but this advantage diminishes rapidly when $\psi > 3$, as ψ increases, and/or as $\tilde{q}$ decreases. As might be intuitively anticipated, the performance of both the ideal PDE and ideal Humphrey cycles approach that of the ideal Brayton cycle as $\tilde{q}$ approaches zero and all heat addition processes approach constant pressure. Of special interest is that the ideal PDE and Humphrey cycles generate useful thermal efficiency in the absence of any mechanical or ram compression whatsoever. Indeed, it is this feature of PDE and/or Humphrey cycles that make them attractive for flight Mach numbers $0 < M_0 < 3$.

Values of $\tilde{q}$ up to about 10 are representative of all hydrocarbon fuels, including hydrogen. Values of ψ correspond either to mechanical compression pressure ratios given by $\pi_c = \psi^{\gamma/(\gamma-1)}$, or to ram compression from a freestream Mach number given by $M_0 = \sqrt{2(\psi - 1)/(\gamma - 1)}$, or some combination thereof, provided that the compression processes are isentropic. For example, for $\gamma = 1.4$, to generate a compression temperature ratio $\psi = 2$, either

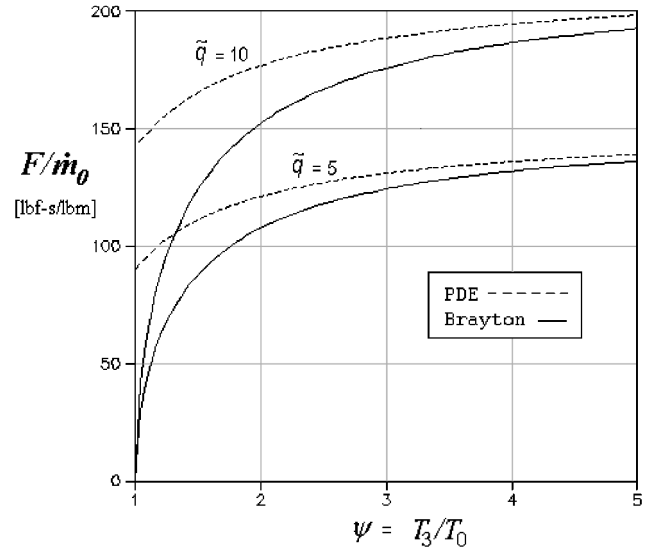

Fig. 5 Specific thrust $F/\dot{m}_0$ of ideal PDE and Brayton cycles as functions of ψ for $\tilde{q} = 5$ and 10 and vehicle speed $V_0 = 0$.

a flight Mach number $M_0 = 2.24$ or a compressor pressure ratio $\pi_c = 11.3$ would be required. Also, when V_0 is greater than zero, then ψ must be greater than 1. For example, when $V_0 = 1000$ ft/s (305 m/s) (corresponding roughly to $M_0 = 1$) the value of ψ is approximately 1.2.

Figures 5–7 illustrate the ideal propulsion performance for the PDE and Brayton cycles under static ($V_0 = 0$) conditions. The results are similar to those for cycle thermal efficiency, except that the square root in Eq. (8) brings the curves close together sooner. The differences between thermal efficiencies for the ideal PDE and ideal Brayton cycles are significant only for $1 < \psi < 2$.

Figures 8–10 illustrate the propulsion performance for ideal PDE and Brayton cycles in forward flight, for a relatively modest flight velocity $V_0 = 1000$ ft/s (305 m/s), corresponding approximately to $M_0 = 1$. The results are similar to those for $V_0 = 0$, except that forward velocity significantly penalizes all performance measures and further reduces the differences between ideal PDE and ideal Brayton performance.

III. Real Thermodynamic Cycle Analysis

The real thermodynamic cycle analysis builds on the platform of ideal cycle analysis by incorporating the effects of any chosen

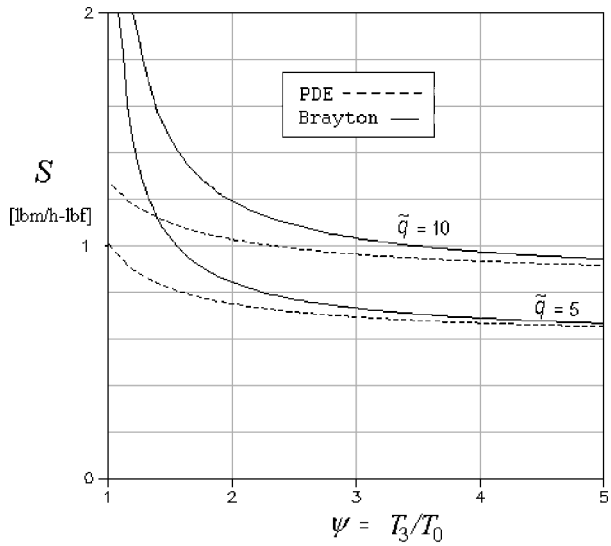

Fig. 6 Specific fuel consumption S of ideal PDE and Brayton cycles as functions of ψ for $\tilde{q} = 5$ and 10, $h_{PR} = 19{,}000$ Btu/lbm, and $V_0 = 0$.

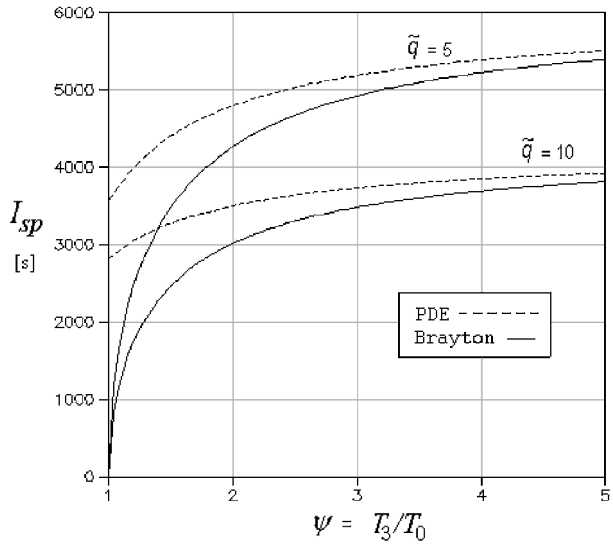

Fig. 7 Specific impulse I_{sp} of ideal PDE and Brayton cycles as functions of ψ for $\tilde{q} = 5$ and 10, $h_{PR} = 19{,}000$ Btu/lbm, and $V_0 = 0$.

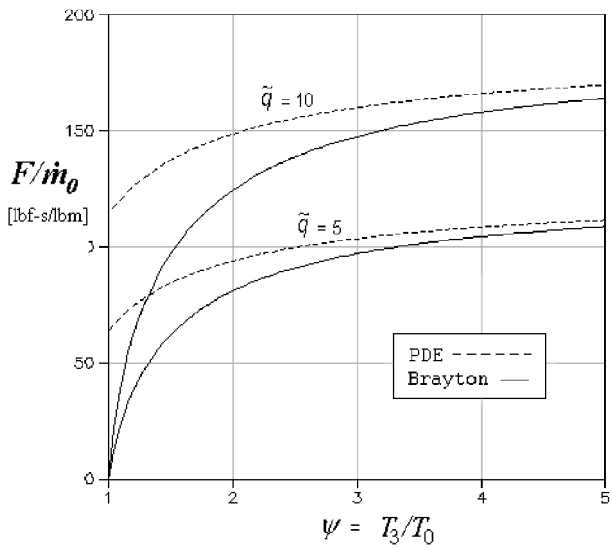

Fig. 8 Specific thrust $F/\dot{m}_0$ for ideal PDE and Brayton cycles as functions of ψ for $\tilde{q} = 5$ and 10 and vehicle speed $V_0 = 1000$ ft/s.

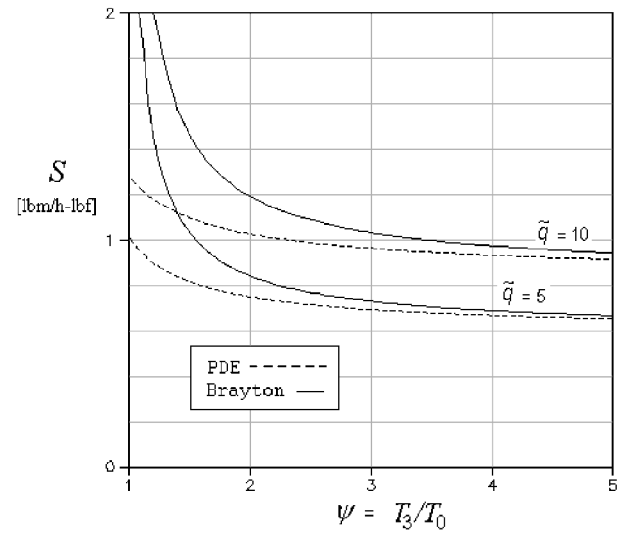

Fig. 9 Specific fuel consumption S for ideal PDE and Brayton cycles as functions of ψ for $\tilde{q} = 5$ and 10, $h_{PR} = 19{,}000$ Btu/lbm, and $V_0 = 1000$ ft/s.

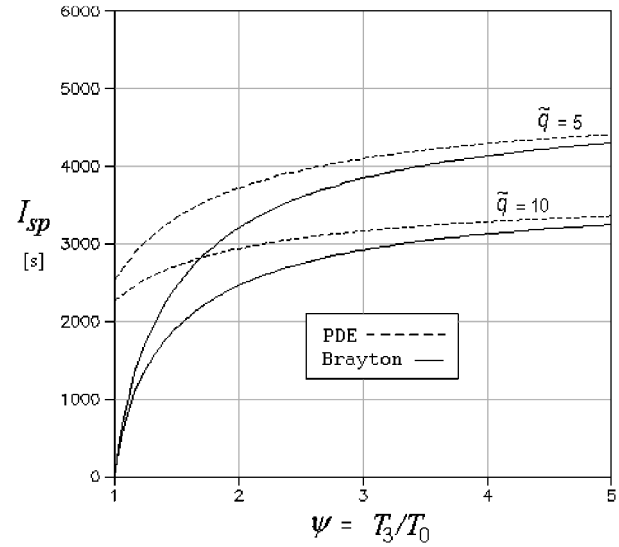

Fig. 10 Specific impulse I_{sp} for ideal PDE and Brayton cycles as functions of ψ for $\tilde{q} = 5$ and 10, $h_{PR} = 19{,}000$ Btu/lbm, and $V_0 = 1000$ ft/s.

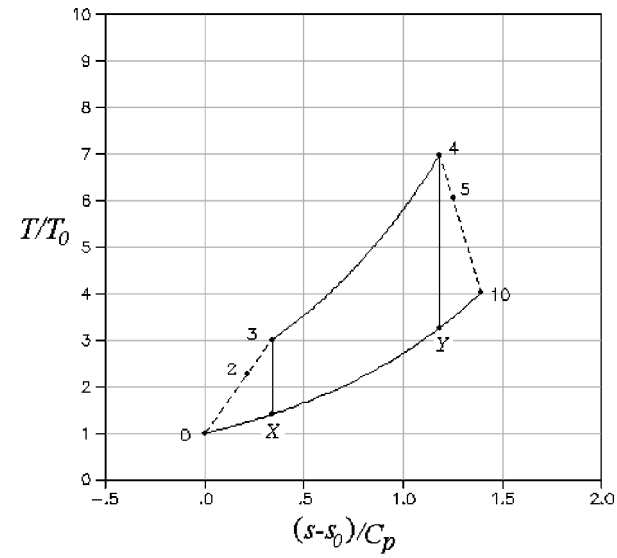

Fig. 11 Temperature–entropy diagram for the real Brayton cycle for $\psi = 3$, $\tilde{q} = 5$, $\eta_c = 0.8$, $\eta_b = 0.8$, and $\eta_e = 0.8$.

irreversibilities. We follow the imaginative and productive path of Builder,[6] as detailed in Ref. 8, although many other avenues are available. Figure 11 contains the additional nomenclature necessary to follow this analysis. Only the alterations to the ideal component processes, which are identical for the PDE, Brayton, and Humphrey cycles, are described below.

From point 0 to point 3, the real compression process is modeled by means of a compression efficiency, which references the actual or real change in static enthalpy to the ideal or isentropic change in static enthalpy that would accompany the same change in static pressure. With reference to Fig. 11, the definition of adiabatic compression process efficiency becomes

$$\eta_c \equiv \frac{h_3 - h_X}{h_3 - h_0} = \frac{C_p(T_3 - T_X)}{C_p(T_3 - T_0)} = \frac{\psi - T_X/T_0}{\psi - 1} \tag{11}$$

From point 3 to point 4, the actual heat addition is reduced because of incomplete combustion to $q_{\text{add}} = \eta_b q_{\text{supp}} = \eta_b f h_{\text{PR}}$, where η_b is the combustion efficiency, f is the mass fuel–air ratio, and h_{PR} is the lower heating value of the fuel.

From point 4 to point 10, the real expansion process is modeled by means of an expansion efficiency, which references the actual or real change in static enthalpy to the ideal or isentropic change in static enthalpy that would accompany the same change in static pressure. With reference to Fig. 11, the definition of adiabatic expansion process efficiency becomes

$$\eta_e \equiv \frac{h_4 - h_{10}}{h_4 - h_Y} = \frac{C_p(T_4 - T_{10})}{C_p(T_4 - T_Y)} = \frac{1 - T_{10}/T_4}{1 - T_Y/T_4} \tag{12}$$

Note that the complexity of expanding the fluid elements generated by the PDE heating/combustion process to local atmospheric pressure will also require special care to establish properly meaningful values of expansion process efficiency for this cycle.

A. Real Brayton Cycle

With standard methods, using the conservation of energy and Gibbs equation for a calorically perfect gas, the thermal efficiency for the real Brayton cycle is[6,8]

$$\eta_{\text{th}} = [(\psi - 1)/\tilde{q}][\eta_c \eta_e (1 + \eta_b \tilde{q}/\psi) - 1] \tag{13}$$

This is a notable closed-form result because it can be differentiated to reveal that, all other quantities than ψ being fixed, the highest value of cycle thermal efficiency occurs at

$$\psi_{\max\eta_{\text{th}}} = \sqrt{\frac{\eta_c \eta_b \eta_e}{1 - \eta_c \eta_e}\tilde{q}} \tag{14}$$

which means that real Brayton cycles have an optimum amount of thermal compression for maximizing the cycle thermal efficiency.

B. Real PDE Cycle

With the standard methods and the definitions of process efficiencies just given, the important state properties around the PDE cycle can be found from the following relationships.

From point 0 to point 3 is the same for all cycles:

$$T_X/T_0 = \psi(1 - \eta_c) + \eta_c \geq 1 \tag{15}$$

$$(s_3 - s_0)/C_p = \ln(T_X/T_0) \geq 0 \tag{16}$$

$$p_3/p_0 = \left[\psi(T_0/T_X)\right]^{\gamma/(\gamma-1)} \geq 1 \tag{17}$$

From point 3 to point 4, the normal shock wave Mach number and total entropy increase are again computed by Eqs. (4) and (5), except that the heat added q_{add} is replaced by $\eta_b\, q_{\text{supp}} = \eta_b f h_{\text{PR}}$:

$$\frac{p_4}{p_0} = \frac{1 + \gamma M_{\text{CJ}}^2}{\gamma + 1}\frac{p_3}{p_0} \geq 1 \tag{18}$$

From point 4 to point 10 is the same for all cycles:

$$T_Y/T_4 = (p_0/p_4)^{(\gamma-1)/\gamma} \leq 1 \tag{19}$$

$$T_{10}/T_4 = 1 - \eta_e(1 - T_Y/T_4) \leq 1 \tag{20}$$

$$(s_{10} - s_4)/C_p = \ln[(T_{10}/T_4)(T_4/T_Y)] \geq 0 \tag{21}$$

From point 10 to point 0 is the same for all cycles:

$$(s_{10} - s_0)/C_p = (s_3 - s_0)/C_p + (s_4 - s_3)/C_p + (s_{10} - s_4)/C_p \tag{22}$$

$$q_{\text{rej}} = h_{10} - h_0 = C_p T_0\{\exp[(s_{10} - s_0)/C_p] - 1\} \tag{23}$$

C. Real Humphrey Cycle

Only the heat addition process differs from the three component processes common to all cycles. The constant-volume heat addition process from point 3 to point 4 results in property changes given by

$$\frac{T_4}{T_3} = 1 + \frac{\eta_b f h_{\text{PR}}}{\psi C_v T_0} = 1 + \frac{\eta_b \tilde{q}\gamma}{\psi} \tag{24}$$

where C_v is the constant-volume specific heat capacity

$$p_4/p_3 = T_4/T_3 \tag{25}$$

$$(s_4 - s_3)/C_p = (1/\gamma)\ln(T_4/T_3) \tag{26}$$

Finally, the real cycle thermal efficiency for all cycles is given by

$$\eta_{\text{th}} = \eta_b \eta_{\text{tc}} = \eta_b(1 - q_{\text{rej}}/q_{\text{add}}) = \eta_b(1 - q_{\text{rej}}/\eta_b q_{\text{supp}}) = \eta_b - q_{\text{rej}}/q_{\text{supp}} \tag{27}$$

Although not as readily expressible in closed form as Eq. (14) for the real Brayton cycle, the real PDE and real Humphrey cycles also exhibit an optimal amount of thermal compression for maximizing the cycle thermal efficiency, as will be illustrated subsequently.

The propulsion performance measures are still computed as for the ideal cycle using Eqs. (8–10). The relative ranking of PDE, Brayton, and Humphrey performance again depends only on η_{th}.

D. Real Thermodynamic Cycle Analysis Results

The specific purpose of this exposition is to evaluate quantitatively the influence of losses on PDE, Brayton, and Humphrey cycles. Therefore, in each case that follows, component process efficiencies will be assumed to be equal for all cycles. Note that all of the η_{th} figures include the ideal PDE, Brayton, and Humphrey cycle results as background for comparison purposes, and that every real PDE, Brayton, and Humphrey cycle performance curve exhibits a maximum, as mentioned earlier for the real PDE and Humphrey cycles and as shown analytically for the real Brayton cycle by Eq. (14).

Figures 12–17 contain the real cycle thermal efficiency results obtained for a number of interesting variations. Figures 12–17 are general in the sense that, provided that the process efficiencies are constant, the results depend only on ψ and $\tilde{q}$, just as in the ideal case. These results emphasize that values of ψ and $\tilde{q}$ must be reported in the literature for analytical or experimental studies to be properly interpreted.

Figure 12 represents the departure point for this exposition. The process efficiencies were chosen to be reasonably attainable in practice while having a sensible impact on performance, and the heat added is about one-half that due to stoichiometric hydrocarbon–air combustion. These results have three special features. First, real performance is considerably less than ideal for all cycles, for all values of ψ. Second, real PDE cycle performance suffers more than the Brayton cycle, so much so that it crosses over and falls below the real Brayton cycle when $\psi > 3$. Third, the real Humphrey cycle performance crosses over and falls below the real Brayton cycle performance when $\psi > 4$. The obvious conclusion is that all three cycles are quite sensitive to losses, especially the PDE cycle, with increasing values of ψ.

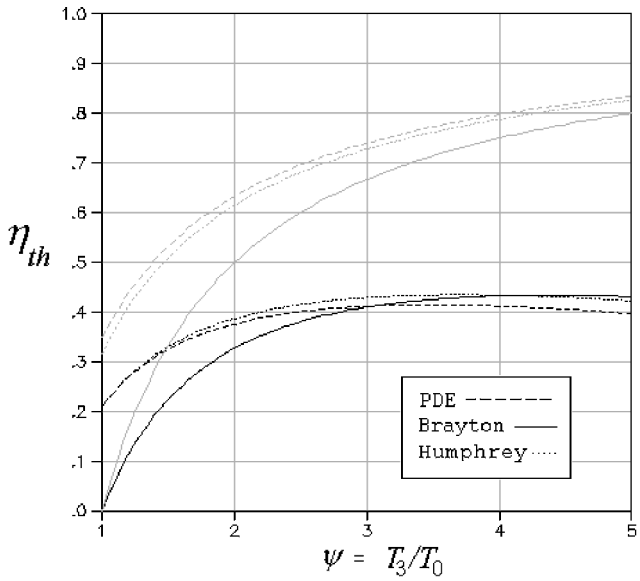

Fig. 12 Thermal efficiency η_{th} of real PDE, Brayton, and Humphrey cycles, as functions of ψ, for $\tilde{q} = 5$, $\eta_c = 0.9$, $\eta_b = 0.9$, and $\eta_e = 0.9$.

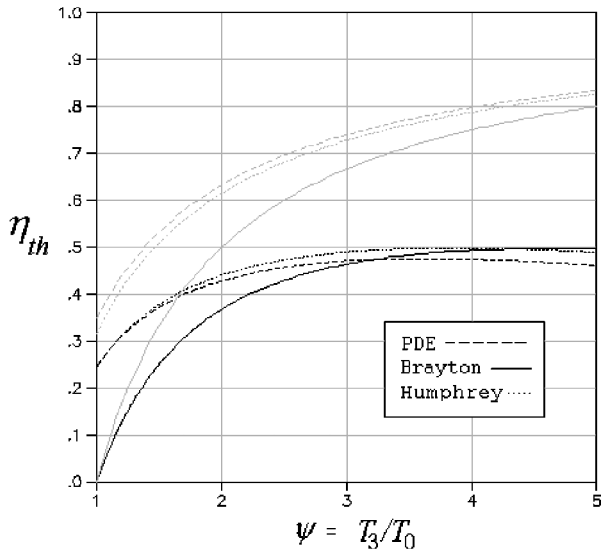

Fig. 13 Thermal efficiency η_{th} of real PDE, Brayton, and Humphrey cycles, as functions of ψ, for $\tilde{q} = 5$, $\eta_c = 0.9$, $\eta_b = 1.0$, and $\eta_e = 0.9$.

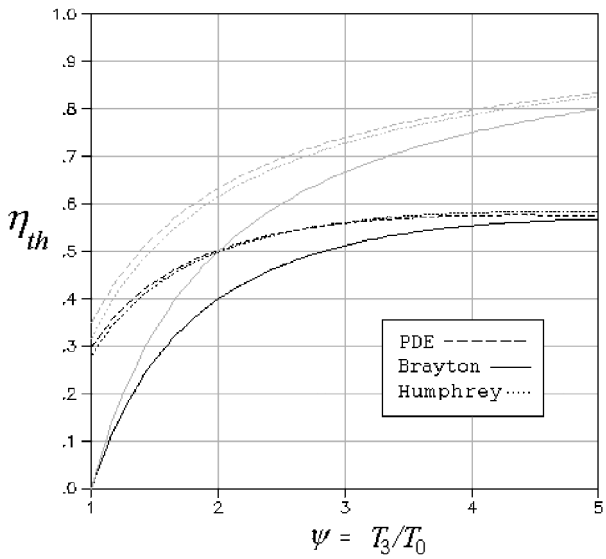

Fig. 14 Thermal efficiency η_{th} of real PDE, Brayton, and Humphrey cycles, as functions of ψ, for $\tilde{q} = 5$, $\eta_c = 0.9$, $\eta_b = 1.0$, and $\eta_e = 0.95$.

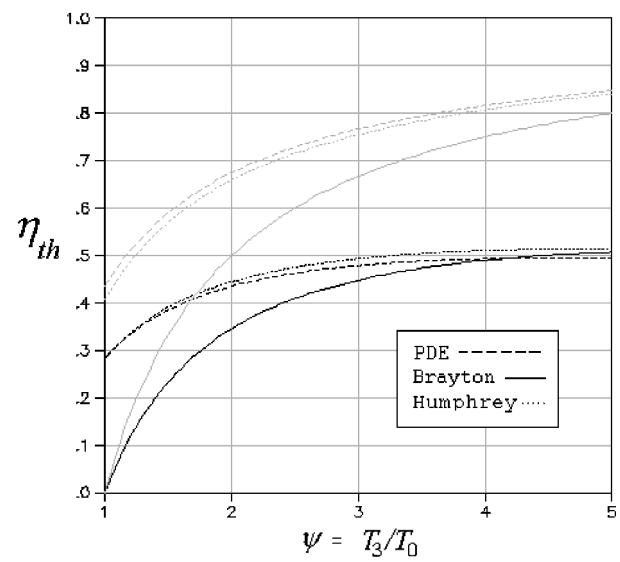

Fig. 15 Thermal efficiency η_{th} of real PDE, Brayton, and Humphrey cycles, as functions of ψ, for $\tilde{q} = 10$, $\eta_c = 0.9$, $\eta_b = 0.9$, and $\eta_e = 0.9$.

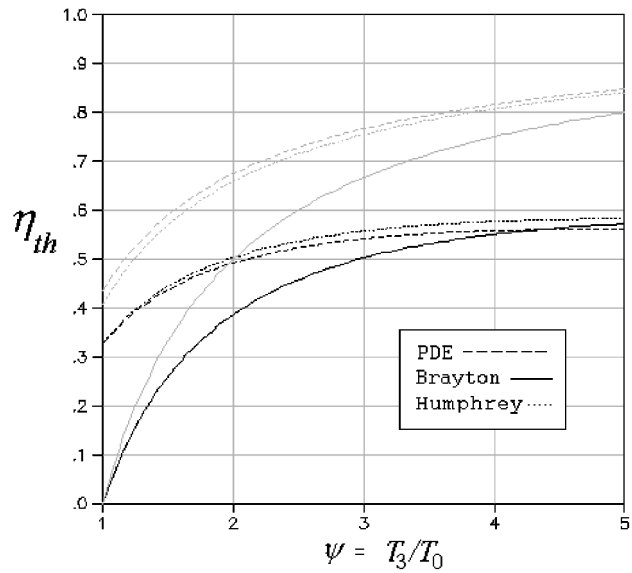

Fig. 16 Thermal efficiency η_{th} of real PDE, Brayton, and Humphrey cycles, as functions of ψ, for $\tilde{q} = 10$, $\eta_c = 0.9$, $\eta_b = 1.0$, and $\eta_e = 0.9$.

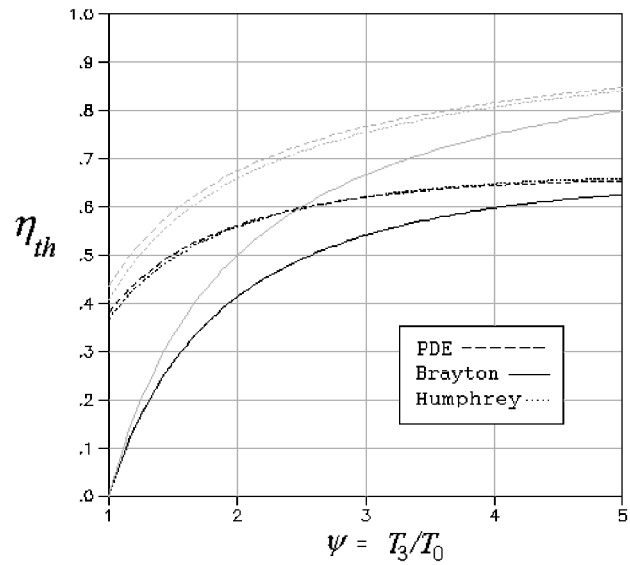

Fig. 17 Thermal efficiency η_{th} of real PDE, Brayton, and Humphrey cycles, as functions of ψ, for $\tilde{q} = 10$, $\eta_c = 0.9$, $\eta_b = 1.0$, and $\eta_e = 0.95$.

Figures 13 and 14 demonstrate the influences of some individual process efficiencies. Comparison of Figs. 12 and 13 reveals, somewhat surprisingly, that significantly increasing the combustion efficiency η_b improves the performance of all cycles, but does not change their relative positions. In particular, the crossover point remains at $\psi \approx 3$ and 4 for the real PDE and real Humphrey cycles, respectively. Comparison of Figs. 12 and 14 reveals that the crossover points appear to be pushed beyond $\psi \approx 5$ when the expansion efficiency η_e is also substantially increased. This is due to the much larger T_4/T_{10} for the PDE cycle vs the Brayton cycle (see Fig. 3) causing the entropy generation for the former from point 4 to point 10 to be more sensitive to η_e. This further emphasizes the earlier noted importance of finding devices that can accomplish this expansion efficiently.

Figures 15–17 repeat the conditions of Figs. 12–14 for increased heat added, approximately equivalent to that due to stoichiometric hydrocarbon–air combustion. Figures 15–17 reveal, in general, that the performance of all three cycles is improved by higher heat release, but that the PDE cycle receives greater benefit than the Brayton cycle and that the Humphrey cycle receives even more. The primary indicator of this effect is that the crossovers are delayed until $\psi > 4$ and 5, respectively. Note that, at near-stoichiometric heat addition, the PDE and Humphrey cycle performance become essentially identical. This analysis can also be applied repetitively to show that compression efficiency is not a prime determinant of differential performance between real PDE and real Brayton cycles. Varying compression efficiency by ±5% changes the difference between their thermal efficiencies by an average of less than ±1% over a wide range of conditions. This is undoubtedly due to the entropy generated in the compression process being identical for the PDE and Brayton cycles in this model. Taken together, the foregoing results underscore the challenge facing PDE designers because the combustion and expansion efficiencies of turbojet engines have been highly refined and are extremely close to one, and ψ is four or more.

Finally, Figs. 18–20 document the effects of losses on propulsion performance measures for the case corresponding to Fig. 12. For reasons already given, the trends parallel those found for cycle thermal efficiency, but the absolute changes are more dramatic, and the effect of forward speed remains substantial.

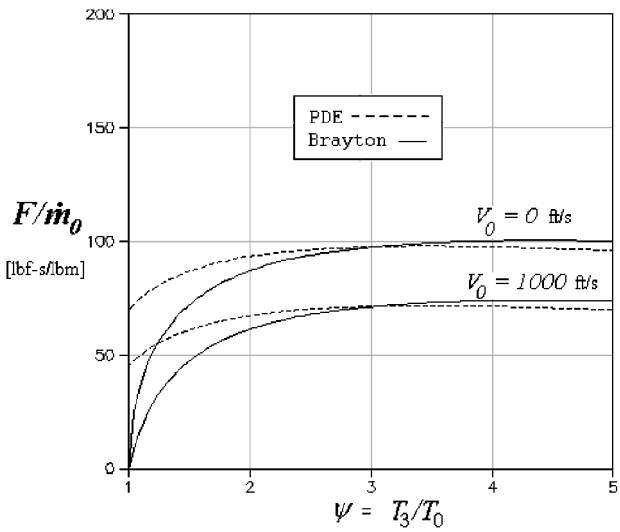

Fig. 18 Specific thrust $F/\dot{m}_0$ for real PDE and Brayton cycles, as functions of ψ, for $V_0 = 0$ and 1000 ft/s, $\tilde{q} = 5$, $\eta_c = 0.9$, $\eta_b = 0.9$ and $\eta_e = 0.9$.

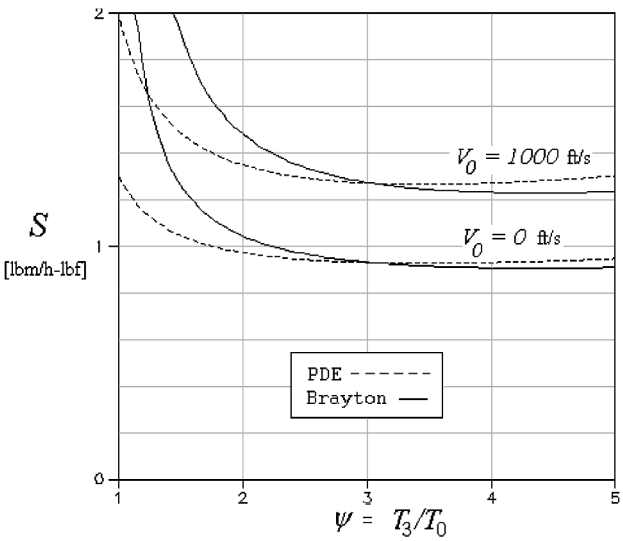

Fig. 19 Specific fuel consumption S for real PDE and Brayton cycles, as functions of ψ, for $V_0 = 0$ and 1000 ft/s, $\tilde{q} = 5$, $\eta_c = 0.9$, $\eta_b = 0.9$, $\eta_e = 0.9$, and $h_{PR} = 19{,}000$ Btu/lbm.

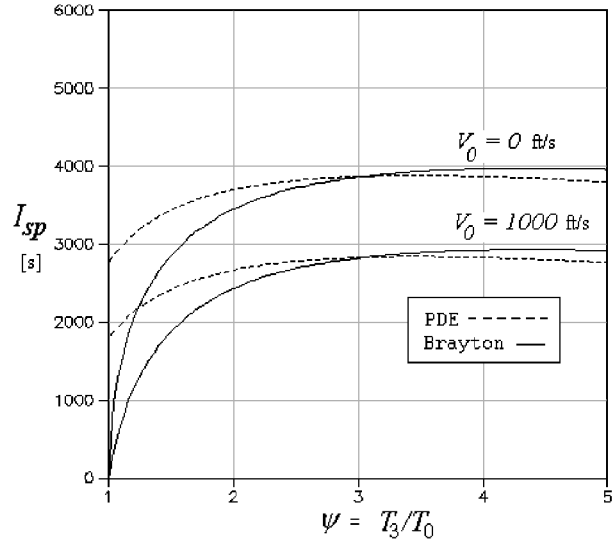

Fig. 20 Specific impulse I_{sp} for real PDE and Brayton cycles, as functions of ψ, for $V_0 = 0$ and 1000 ft/s, $\tilde{q} = 5$, $\eta_c = 0.9$, $\eta_b = 0.9$, $\eta_e = 0.9$, and $h_{PR} = 19{,}000$ Btu/lbm.

IV. Conclusions

The ideal thermodynamic cycle efficiency of the PDE is in the range of 0.4 to 0.8 for typical hydrocarbon fuels (see Fig. 4), corresponding to an I_{sp} in the range of 3000 to 5000 s (see Fig. 7). This exceeds the ideal thermodynamic efficiency of the Brayton cycle under all conditions, especially near static conditions where the Brayton cycle has little cycle static temperature ratio.

For realistic but equal component process efficiencies, real PDE thermodynamic cycle efficiency continues, for the same reason, to be superior to that of the real Brayton cycle near static conditions. However, real PDE cycle performance falls off more rapidly than the real Brayton cycle, and can be inferior beyond $\psi \sim 3$ (see Figs. 12–17), corresponding either to isentropic ram compression from $M_0 \sim 3$ or isentropic mechanical compression with pressure ratio $\pi_c \sim 46$. The expected I_{sp} of real PDE cycles using typical hydrocarbon fuels is in the range of from 2000 to 4000 s (see Fig. 20).

Utilizing the Humphrey cycle as a surrogate for the PDE cycle has some surprising consequences. Because the ideal Humphrey cycle has a thermal efficiency just slightly less than the ideal PDE cycle, (see Fig. 4) this substitution would appear to be conservative. However, when realistic component process efficiencies are considered, the real Humphrey cycle thermal efficiency remains comparatively high with increasing compression, while the real PDE thermal efficiency falls off significantly.

With the methodology presented in this paper, it is possible to carry out further sensitivity studies of one's own choice, or to modify this analysis to improve or add loss models, as generations of propulsion engineers have long done. Moreover, the building block model

for PDE combustion presented here can be inserted into propulsion cycles of increasing complexity to obtain qualitative insight and quantitative estimates. Finally, the computed results provide indicators of the expected performance of PDE devices and how that performance may be improved.

Acknowledgments

The authors wish to thank Louis A. Povinelli and Gerard Welch of the NASA John H. Glenn Research Center at Lewis Field for providing financial support for the work and for stimulating our interest and involvement in this topic.

References

[1]Bussing, T. R. A., and Pappas, G., "Pulse Detonation Engine Theory and Concepts," *Developments in High-Speed Vehicle Propulsion Systems*, edited by S. N. B. Murthy and E. T. Curran, Vol. 165, Progress in Aeronautics and Astronautics, AIAA, Reston, VA, 1996, pp. 421–472.

[2]Kailasanath, K., "Applications of Detonations to Propulsion: A Review," AIAA Paper 99-1067, Jan. 1999.

[3]Cambier, J.-L., and Tegner, J. K., "Strategies for Pulsed Detonation Engine Performance Optimization," *Journal of Propulsion and Power*, Vol. 14, No. 4, 1998, pp. 489–498.

[4]Eidelman, S., and Yang, X., "Analysis of the Pulse Detonation Engine Efficiency," AIAA Paper 98-3877, July 1998.

[5]Sterling, J. D., Ghorbanian, K., Humphrey, J. W., Sobota, T. H., and Pratt, D. T., "Numerical Investigations of Pulse Detonation Wave Engines," AIAA Paper 95-2459, July 1995.

[6]Builder, C. H., "Thermodynamic Spectrum of Airbreathing Propulsion," AIAA Paper 64-243, June 1964.

[7]Oates, G. C., *Aerothermodynamics of Gas Turbine and Rocket Propulsion*, AIAA Education Series, 3rd ed., AIAA, Washington, DC, 1997, pp. 121–151.

[8]Heiser, W. H., and Pratt, D. T., *Hypersonic Airbreathing Propulsion*, AIAA Education Series, AIAA, Washington, DC, 1994, pp. 109–119, 149–173.

[9]Strehlow, R. A., *Combustion Fundamentals*, McGraw–Hill, New York, 1984, pp. 127–138, 302–307.

[10]Shapiro, A. H., *The Dynamics and Thermodynamics of Compressible Fluid Flow*, Ronald, New York, 1953, pp. 193–211.

[11]Pratt, D. T., Humphrey, J. W., and Glenn, D. E., "Morphology of Standing Oblique Detonation Waves," *Journal of Propulsion and Power*, Vol. 7, No. 5, 1991, pp. 837–845.